High Power Laser Science and Engineering, (2024), Vol. 12, e22, 8 pages.
doi:10.1017/hpl.2024.13

HIGH POWER LASER SCIENCE AND ENGINEERING

RESEARCH ARTICLE

A multi-shot target wheel assembly for high-repetition-rate, laser-driven proton acceleration

J. Peñas[1,†], A. Bembibre[1,†], D. Cortina-Gil[1], L. Martín[2], A. Reija[1], C. Ruiz[3], M. Seimetz[4], A. Alejo[1], and J. Benlliure[1]

[1]*Instituto Galego de Física de Altas Enerxías, Universidade de Santiago de Compostela, Santiago de Compostela, Spain*

[2]*Laboratorio Láser de Aceleración y Aplicaciones, RIAIDT, Universidade de Santiago de Compostela, Santiago de Compostela, Spain*

[3]*Instituto Universitario de Física Fundamental y Matemáticas y Dpto. de Didáctica de la Matemática y de las Ciencias Experimentales, Universidad de Salamanca, Salamanca, Spain*

[4]*Instituto de Instrumentación para Imagen Molecular (I3M), CSIC-Universitat Politècnica de València, Valencia, Spain*

(Received 3 February 2024; revised 22 February 2024; accepted 8 March 2024)

Abstract

A multi-shot target assembly and automatic alignment procedure for laser–plasma proton acceleration at high repetition rate are introduced. The assembly is based on a multi-target rotating wheel capable of hosting more than 5000 targets, mounted on a 3D motorized stage to allow rapid replenishment and alignment of the target material between laser irradiations. The automatic alignment procedure consists of a detailed mapping of the impact positions at the target surface prior to the irradiation that ensures stable operation of the target, which alongside the purpose-built design of the target wheel, enables operation at rates up to 10 Hz. Stable and continuous laser-driven proton acceleration at 10 Hz is demonstrated, with observed cut-off energy stability about 15%.

Keywords: high repetition rate; laser–plasma acceleration; multi-shot operation; proton source; target assembly

1. Introduction

The acceleration of ions from the interaction of a high-power laser with a plasma has attracted growing interest over the last two decades[1,2]. Efficient acceleration of light ions can be achieved through a variety of established and emerging accelerating mechanisms, whose dominance depends on the laser and target characteristics. Arguably, the so-called target normal sheath acceleration (TNSA) mechanism is the most-established and robust route to accelerate light ions to multi-MeV energies[3,4]. In TNSA, the laser interacts with an overdense plasma, typically generated by the pedestal preceding the main pulse in high-power systems. During the interaction, a large number of fast electrons from the front surface are driven into the target. These fast electrons will reach the target rear surface, where a fraction will leave the target and generate a quasi-electrostatic, capacitor-like field at the rear surface, with values of the order of TV m^{-1}. Such a strong electric field will ionize the atoms on the rear surface and accelerate the ions to multi-MeV energies. The TNSA-driven ion beams are characterized by their multi-species nature, but dominated by protons, with quasi-exponential spectra extending up to a sharp cut-off energy that scales with the laser intensity as $E_{\mathrm{ion}} \propto I^{0.5-0.7}$[2] and emitted with a divergence of up to tens of degrees.

Parallel to the studies of laser-driven ion acceleration, there has been significant progress in laser technology, not only towards achieving increasingly larger powers, but also towards the development of multi-TW laser systems with increasingly higher repetition rates. The advent of these multi-hertz high-power laser systems is leading to a growing need for novel target systems capable of operating at such rates. Due to the destruction of the target following the interaction with the laser, an appropriate system needs to be capable of replenishing the target and positioning it on the focal plane of the laser with micrometre-level precision, as given by the Rayleigh length for the short f-number optics used in this type of experiment. Furthermore, a future laser-based ion accelerator will be required to operate continuously at these rates for extended periods of time, and therefore a suitable target system must be able to host thousands of targets.

Correspondence to: A. Alejo and J. Benlliure, Instituto Galego de Física de Altas Enerxías, Universidade de Santiago de Compostela, Santiago de Compostela 15705, Spain. Email: aaron.alejo@usc.es (A. Alejo); j.benlliure@usc.es (J. Benlliure)

[†]These authors contributed equally to this work.

Several alternatives are being actively studied as potential target systems[5]. Some promising recent developments include the use of liquid targets[6], liquid crystal targets[7,8], high-density gas jets[9,10] and cryogenic solid hydrogen targets[11,12], all of which would ensure the operation for extended periods of time. However, these solutions still face major challenges, such as the shape and profile manipulation, micrometric positioning and restrictions in operation due to the high-vacuum level required by the laser systems. For these reasons, target systems based on the replenishment of foil-based solid targets remain as the most common solution, typically in the form of tape-drive systems or multi-target holder systems.

Tape-drive-based targets allow for tens of thousands of shots, which at 10 Hz would correspond to almost 1 h of continuous operation[13–16]. The main drawback of these systems is the limited variety of tape materials and thicknesses suitable to withstand the mechanical stress caused by the continuous movement. In this context, multi-target holder systems appear as an appealing alternative, thanks to the flexibility of using a rigid structure to support the target foils, allowing for a broad variety of suitable target materials and thicknesses[17]. However, these configurations present two major limitations, namely the relatively reduced number of shooting positions, typically hosting fewer than 1000 targets; and the reduced repetition rate at which they can be operated, due to the need to replace and realign with micrometre-level precision after each irradiation. Recent developments have tried to tackle these limitations in order to extend the usability of multi-target holder systems.

In order to increase the number of targets, Gao *et al.*[17] proposed a system based on a metallic target wheel hosting target plates accommodating up to approximately 1700 impact positions. However, the maximum operation rate of this target assembly is limited to 0.5 Hz, as given by the relaxation time to reduce the vibrations of the target wheel after the movement of the motorized stages. Another appealing alternative to increase the shooting positions is the use of micro-electromechanical system (MEMS) technology to fabricate micro- and nano-targets on silicon wafers[18–20]. This technology allows for manufacturing large volumes of micro-targets made of different materials and thicknesses, including composites of various distinct layers. For instance, Gershuni *et al.* [20] propose a target delivery system based on 100-mm-diameter Si wafers where hundreds of micro-targets can be created using MEMS technology. However, the online measurement and closed-loop correction sequence for target realignment limited the repetition rate to 0.2 Hz.

Here we report on a multi-shot target assembly based on a rotating wheel capable of hosting more than 5000 targets, which is compatible with operation at a repetition rate of 10 Hz. Furthermore, we describe the procedure implemented to ensure automatic shot-to-shot replenishment and realignment of each target at 10 Hz, based on a few-minute measurement for the pre-characterization of the shooting positions with a high-precision industrial sensor, which allows for the positioning of the targets on the focal plane with a precision of $\sigma = 3.5$ μm. Experimental results on laser-driven ion acceleration from the developed target and alignment method at the Laser Laboratory for Acceleration and Applications (L2A2)[21,22] are presented, demonstrating stable, continuous operation for more than 1000 shots with deviations in the cut-off energy of the measured proton spectra of approximately 15%, limited by the stability of the laser system. The rest of the paper is structured as follows. The target assembly, including a detailed description of the design requirements for the target wheel depending on the stages and minimum repetition rate, is included in Section 2. The target pre-mapping and automatic positioning procedure are described in Section 3. Finally, the experimental setup and results of ion acceleration using the rotating wheel target are discussed in Section 4.

2. Multi-shot target assembly

The target assembly developed is based on a multi-shot rotating wheel attached to a 3D motorized rig to ensure the shot-to-shot replacement and positioning of the target material (Figure 1(a)). The motorized rig consists of a rotational stage (PimiCos T-65N) that enables the rotation of the target wheel around its axis (ϑ); a linear stage (PimiCos DT-65N) that enables the translation along the target normal, or longitudinal direction (z); and a linear stage (PimiCos LS-110) that enables the translation along the direction perpendicular to the target normal, or radial direction (r). The combined motion of the rotational and radial stages allows one to change the irradiated target between laser shots, whereas a combined motion of the radial and longitudinal stages allows one to displace the wheel along the laser focal direction and position each target at the focal plane. The spatial resolutions of the rotational, longitudinal and radial stages are 20 μdeg, 10 nm and 20 nm, respectively, significantly lower than the required tolerance for the positioning of the target at the focal plane, typically of the order of 10 μm (see Section 3).

The key element of the target assembly is the multi-shot rotating wheel. In our case, the wheel is formed by a base 304-mm-diameter, 2-mm-thick aluminium disk that can be directly attached to the rotational stage, and is capable of hosting up to eight target sectors. The material and thickness of the disk are a compromise between minimizing the overall weight, below the maximum load for the stages, while maximizing the stability and robustness of the structure. Each sector consists of a target foil of choice sandwiched between two planar plates of 400 μm in thickness, with pre-drilled holes that allow the irradiation of the target by the laser (Figure 1(b)). These planar plates allow one to ensure the stability of the foil throughout the operation, avoiding the deformation of the foil in impact positions adjacent to the

https://doi.org/10.1017/hpl.2024.13 Published online by Cambridge University Press

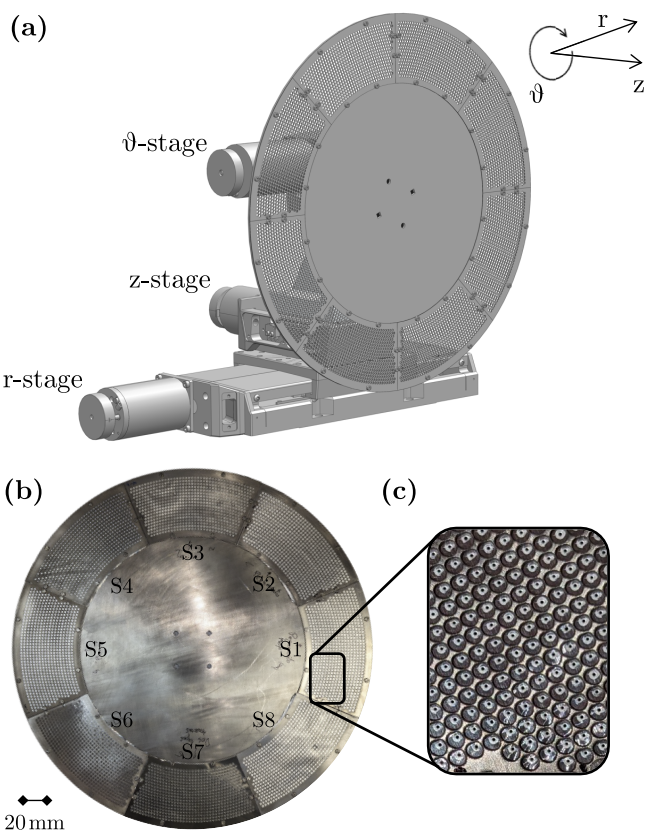

Figure 1. (a) Drawing of the target assembly, depicting the three motorized stages and a rotating wheel. (b) Picture of a target wheel design for 10 Hz operation. (c) Zoomed-in picture of the target wheel, showing the craters on the targets after their irradiation.

irradiated targets (Figure 1(c)), which could otherwise result in changes greater than 100 μm. The actual distribution, which sets the maximum repetition rate and number of impact positions of the wheel, is limited by factors such as the maximum speed and range of motion of the stages, as well as the minimum size of and distance between the holes on the sector plates. In order to maximize the number of irradiation points, the pre-drilled holes are distributed along concentric circular patterns, where the diameter of each hole is kept at 2 mm to prevent damage by the laser. The flexibility of the design ensures its compatibility with a broad range of target materials and thicknesses (see Supplemental Material for additional details). Given the thinness of the plates, a minimum centre-to-centre distance between holes of $d_H = 2.5$ mm was required in order to ensure mechanical stability.

Considering the aforementioned constraints, the maximum repetition rate of operation of the target for a row of the circular pattern at radius R_H is limited by the maximum velocities for the rotational ($\dot{\vartheta}_{max} = 22$ deg s^{-1}) and radial ($\dot{r}_{max} = 25$ mm s^{-1}) stages. In our case, a key requirement for the wheel is its capability to operate at 10 Hz, resulting in a maximum target-replacement time of $\tau_R = 100$ ms. Therefore, the impact positions must verify that $d_H \leq \tau_R/\dot{r}_{max} = 2.5$ mm and $d_H \leq R_H\,\dot{\vartheta}_{max}\,\tau_R = 0.038R_H$. In addition to setting a maximum centre-to-centre distance between holes, already fulfilled by our wheel design, these conditions establish a minimum radius for the circular pattern of holes, corresponding to $R_H \geq 65$ mm for our conditions. However, it should be noted that larger radii will result in a greater number of impact positions. For this reason, the inner radius in our case was designed to be 100 mm, whereas the number of concentric arcs was limited to 18, as given by the centre-to-centre inter-hole distance and the range of motion of the radial stage (50 mm). As a result, each sector can host up to 650 targets, leading to a total of 5200 targets for the entire wheel. Such a large number of shooting positions not only represents a significant increase with respect to similar systems based on multi-target holders[17,23], but also makes this design competitive with respect to other solutions, such as tape-drives or MEMS targets, particularly considering that it can be further increased through careful choices of the inner and outer radii of the shooting positions.

3. Target automatic positioning system

The tolerance for the target positioning is defined by the length in which the laser beam remains focused, given by its Rayleigh length, typically of the order of approximately 10 μm for the focusing optics employed in laser-driven ion acceleration experiments. This accuracy is beyond the intrinsic precision of the target system, limited by factors such as mechanical deformations of the wheel and target foil, or the wobbling associated with the rotational stage. Therefore, some form of positioning system is required in order to ensure the placement of each target on the focal plane without the need for individual alignment.

In our case, we have implemented an automatic correction system based on adjusting the target position according to a detailed 3D mapping of the impact positions of the laser pulses on the target, allowing for operation at higher repetition rates than other methods based on online, live correction procedures. To obtain this pre-map, the coordinates of the desired impact positions on the target wheel are defined by its mechanical design, while the longitudinal coordinate, or displacement along the target normal, is measured with an OptoNCDT ILD1320 position sensor by Micro-Epsilon, with a reproducibility of 1 μm (Figure 2). It should be noted that the sensor cannot operate in vacuum, and therefore the entire wheel characterization must be performed in atmospheric conditions prior to the irradiation. In order to perform the characterization in similar conditions to those found during the irradiation, the process is performed at a rate of 10 points per second, which for our 5200-target design corresponds to an entire wheel being evaluated in less than 9 min, which could be further reduced by performing the pre-characterization at the maximum speed of the

https://doi.org/10.1017/hpl.2024.13 Published online by Cambridge University Press

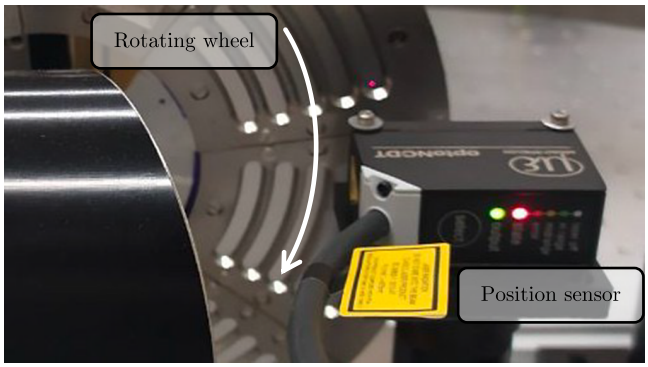

Figure 2. Picture of the setup used for the validation of the target positioning system.

different motorized stages. Our method represents a significant improvement with respect to conventional target characterization techniques, for example, the 100 min required to characterize 1000 impact positions by Chagovets *et al.*[23].

A pre-map measured using the distance sensor for the wheel in Figure 1(b) is shown in Figure 3(a). Large deviations can be observed between the different shooting positions, with variations greater than 1 mm between different regions of the wheel. Furthermore, these deviations are measured not only between different sectors, but also between consecutive targets within the same sector, indicating a deformation of the target surface probably caused by the procedure to sandwich the target foil between the pre-drilled plates, as pointed out by the greater deviations in the regions away from the edges where the target foil is clamped.

The information contained in the pre-map can be subsequently used to automatically correct the position of each target. In our case, a control software was developed using LabVIEW to handle the motion of the three motorized stages in the target assembly. In the first step, the system calculates the initial deviation with respect to the desired plane for each impact position, as shown in Figure 3(b) (black line). This information is used to calculate the required combined motion of the stages in order to place the target at the desired plane while ensuring that the impact position remains unchanged.

To validate this technique, a position verification was performed, based on the measurement by the distance sensor of the displacement of the impact positions while the correction was being applied. This process was performed in the same conditions as the real laser irradiations, including the equivalent motion profile for the different stages and operation at a repetition rate of 10 Hz. The results of this procedure for the first approximately 1000 impact positions are shown in Figure 3(b) (red), which clearly indicate an improvement with respect to the original movements without correction. For clarity, the same results are shown with a different scale in Figure 3(c), where the individual measurements by the sensor are depicted by the markers, and the straight line

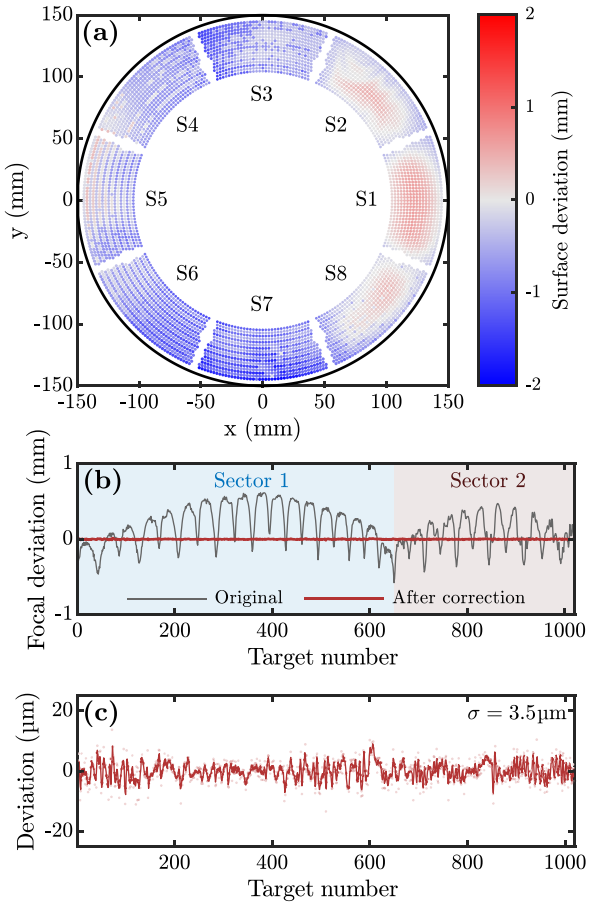

Figure 3. (a) 3D surface map of the aluminium target foils installed at the multi-target wheel. (b) Surface profile of the first approximately 1000 impact positions before (black curve) and after (red curve) correction. (c) Zoomed-in view of the deviation of the impact positions after the correction shown in (b). Each impact position appears represented by an individual marker, and the straight line shows the 3-point moving average of the deviations.

represents a 3-point moving average of the experimental data. The distribution of measurements shows a standard deviation of $\sigma = 3.5$ μm, well below the Rayleigh length of the laser system, and a maximum deviation of 13.7 μm. Considering a Gaussian beam focused using $f/3$ optics, the standard deviation leads to the peak intensity varying in the range of 92%–100%, and a maximum intensity drop for the maximum deviation to 46% of the peak intensity. To confirm the robustness and accuracy of the procedure, the surface map before and after correction was repeatedly measured, with different measurements being in good agreement at the micrometre level, supporting the repeatability of the method.

It should be noted that, although the developed control system has been shown to be capable of accurately positioning each target at the desired plane, it is crucial to ensure that such a plane corresponds to the focal plane of the laser beam. In our case, this information is fed into the control system by manually bringing one of the targets to the laser focal plane. Different techniques are available for the alignment

https://doi.org/10.1017/hpl.2024.13 Published online by Cambridge University Press

of solid targets, such as the speckle technique[24], the retro-imaging technique[25,26] and the direct imaging technique[27]. For the results here presented, the latter was used, in which the focal plane of the laser is initially found with a high-magnification imaging system, allowing one to place a back-illuminated target at the same plane by ensuring the same optical system is imaging the rear surface of the target. It should be noted that the imaging system used to establish the reference position was also employed to confirm the validity of the pre-map in vacuum conditions, as well as the lack of deformation of the surface of the surrounding shooting positions after the irradiation of any given target.

4. Proton acceleration at the Laser Laboratory for Acceleration and Applications

4.1. Experimental setup

Laser-driven proton acceleration using the developed rotating wheel target and automatic alignment procedure has been studied experimentally at 10 Hz using the setup schematically depicted in Figure 4. The experiments were performed utilizing the STELA laser system, hosted at the L2A2 (Universidade de Santiago de Compostela)[21,22], which provided p-polarized, 800 nm-wavelength pulses at a repetition rate of 10 Hz, containing energies of up to 0.3 J on target, and compressed to a duration of approximately 40 fs.

Inside a vacuum chamber maintained at a pressure of approximately 1×10^{-6} mbar, the laser beam was focused onto the targets with a 45° off-axis parabolic mirror (f/2.8) down to an approximately 5 μm focal spot size (full-width-at-half-maximum), reaching intensities of approximately 3×10^{19} W cm^{-2} and corresponding to a 24-μm Rayleigh length. Aluminium foils of 12-μm thickness were mounted on the rotating target wheel and used as targets. The aforementioned procedure was employed for the replacement and positioning of the targets on the focal plane. The automatic control system was synchronized with the laser through a common trigger in order to ensure that each movement was completed between the irradiations.

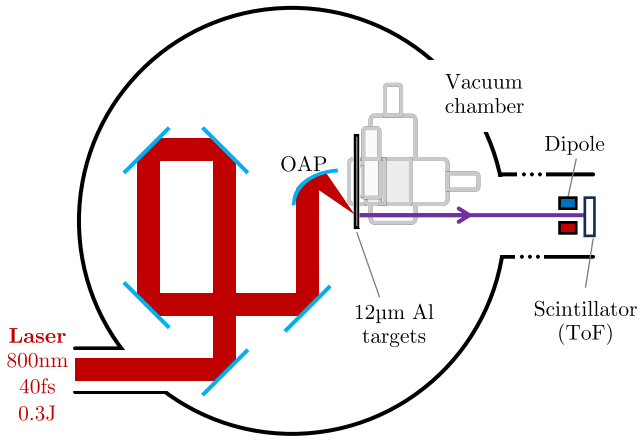

Figure 4. Schematic representation of the experimental setup used at the L2A2.

The laser-driven proton beam was characterized using the time-of-flight (ToF) technique, based on the temporally resolved measurement of the signal produced by the protons reaching a detector placed at a distance of 2 m from the interaction point. In order to prevent the detection of electrons, a dipole magnet was placed along the path to deviate electrons while allowing ions and photons into the detector. The detector consisted of a fast plastic scintillator (NE102A) covering an area of 25 mm × 25 mm (∼0.16 msr), with a thickness of 5 mm, sufficient to stop incoming protons with energies up to 22.5 MeV. In order to reduce the external light noise in the detection system, the scintillator piece was covered by a (4 ± 1)-μm-thick layer of aluminized Mylar. Considering the variations in the filter thickness, the minimum proton energy detectable is 300 keV, with a partial, nonlinear transmission extending up to 500 keV. The signal emitted by the scintillator was collected and detected using a photo-multiplier tube (PMT). In order to minimize the electromagnetic noise caused by the laser–plasma interaction, the PMT was shielded and placed away from the radiation by means of optical fibres for its coupling with the scintillator. Due to the large optical signals generated in the scintillator, a neutral density filter OD1 was placed between the optical fibres and the PMT[28].

4.2. Experimental results

The ToF signal measured for 1032 consecutive shots, corresponding to the mapped target points in Figures 3(b) and 3(c), is shown in Figure 5(a), where the line and shaded area represent the average and the standard deviation of the signals, respectively. Two distinct peaks can be identified on the signal. The first peak corresponds to the so-called gamma flash, produced by high-energy photons generated during the laser–plasma interaction, which can be used as a reference time for the arrival of the laser pulses. The second peak in the signal corresponds to the incoming charged particles, protons and heavier ions reaching the scintillator at a later time depending on their energy E_i.

The energy spectrum of the ion beam can be reconstructed from the ToF signal. Considering the non-relativistic limit, the detection time and energy can be related through the following expression:

$$E_i = \frac{1}{2} m_i \left(\frac{D}{\Delta t_i + D/c} \right)^2, \tag{1}$$

where m_i is the ion mass, D is the length of the flight path, c is the speed of light and Δt_i is the delay of the signal with respect to the arrival of the gamma flash. It should be

https://doi.org/10.1017/hpl.2024.13 Published online by Cambridge University Press

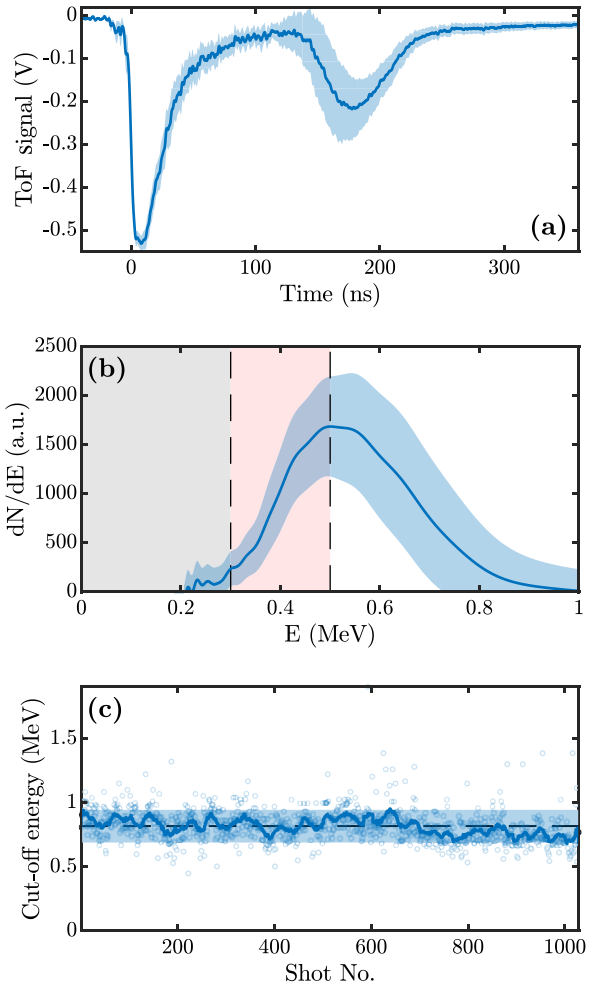

Figure 5. (a) Time-of-flight signal of the laser-driven ions. The line and shaded area represent, respectively, the average and standard deviation of the signal detected for 1032 consecutive shots obtained at 10 Hz. (b) Energy spectrum obtained for the data in (a). The black and red shaded areas indicate the proton energies not transmitting and those partially transmitted with nonlinear transmission, respectively. (c) Evolution of the proton cut-off energy, where each individual marker indicates the peak energy for each irradiation; the dark line shows the 20-period moving average and the shaded area shows the standard deviation of the cut-off energies around the 0.81 MeV mean energy.

noted that, as previously discussed, laser-driven ion beams are characterized by having a multi-species nature, but are heavily dominated by protons from the contaminant layers on the target surface, and to a lesser extent by carbon and oxygen ions. Unlike other diagnostic tools, such as Thomson parabola spectrometers, ToF-based diagnostics cannot discriminate between different ion species. However, given the dominance of the protons within the beam, as well as the presence of the aluminized Mylar capable of fully stopping carbon and oxygen ions with energy up to approximately 2.6 MeV, it will be assumed that the ToF signal is produced only by protons. The mean proton spectrum and standard deviation retrieved from the ToF signals are shown in Figure 5(b), where the black and red shaded areas indicate the aforementioned regions of no-transmission and partial, nonlinear transmission by the filter, respectively.

In order to quantify the stability and reproducibility of the ion source, the proton cut-off energy has been extracted from the reconstructed proton spectra, shown in Figure 5(c), where the individual markers represent the cut-off energy for each individual irradiation, and the straight line depicts the 20-point moving average of the data. As can be seen, the points are distributed around a mean cut-off energy of 0.82 MeV, with a dispersion given by the standard deviation of 0.12 MeV, representing approximately 15% of relative dispersion. Although these values support the high reproducibility and stability of the long-term operation of the target wheel and proton source, the dispersion is larger than what would be expected considering the measured reproducibility of the target positioning on the focal plane. However, it should be noted that this variability is identical to that found from the irradiation of manually aligned targets under identical experimental conditions. In particular, an average energy of approximately 0.7 MeV and standard deviation of 0.1 MeV were measured from the irradiation of 70 targets, leading to a 15% dispersion (see Supplemental Material for further details). Therefore, we conclude that the fluctuations of the ion spectra and cut-off energy arose from differences during the laser–plasma interaction. Considering that the different parameters of the laser, such as energy, pointing and spatial phase, were not stabilized, the evolution of these parameters could be partially responsible for the observed variability of the ion spectra. Furthermore, the continuous irradiation of the laser results in the heating of the different optical elements along the beamline, which has been shown to rapidly affect the alignment and behaviour of the laser, in turn degrading the stability of the proton beam[22].

5. Conclusions

Here we have presented a multi-shot target assembly for laser–plasma ion acceleration compatible with multi-hertz operation. The assembly consists of a 3D motorized rig, with one rotational and two linear stages that guarantee the shot-to-shot replenishing and positioning at laser focus of the target material, and a wheel target holder. The rotating wheel is capable of hosting more than 5000 targets and is designed to operate continuously at rates of up to 10 Hz.

An automatic procedure for the alignment of the target surface with respect to the laser focal plane for each impact position has been introduced. This procedure is based on a 3D pre-map of the desired shooting positions obtained prior to irradiation, with an industrial optical sensor with micrometre-level precision. This map of positions, which can be retrieved in a few minutes, can be used to calculate the required correction to ensure the target placement by the software controlling the shot-to-shot movement of the three stages of the target assembly. Following this procedure,

https://doi.org/10.1017/hpl.2024.13 Published online by Cambridge University Press

we have demonstrated that the individual targets can be positioned at the laser focus with an accuracy of $\sigma = 3.5\ \mu$m, significantly lower than the approximately 10 μm precision required due to the Rayleigh length of the focusing system. This solution represents a significant boost in both the number of shots, competitive with respect to other solutions such as MEMS technology or tape-drive systems, and the repetition rate at which it can operate, without requiring prolonged periods for the manual pre-characterization of the target surface.

The target assembly has been successfully used to accelerate ions using the high-power laser system at the L2A2 facility. The laser-driven proton beam has been characterized by means of a ToF detector. A stable, continuous, 10 Hz laser-driven proton source was demonstrated from the irradiation of more than 1000 consecutive targets, exhibiting a mean cut-off energy of 0.82 MeV and relative dispersion of 15%, probably due to the shot-to-shot variations in the laser parameters.

Supplementary material

The supplementary material for this article can be found at http://doi.org/10.1017/hpl.2024.13.

Acknowledgements

This work was supported by the Spanish Ministerio de Ciencia, Innovación y Universidades under grants RTI2018-101578-B-C21, RTI2018-101578-B-C22, FPI predoctorals BES-2017-08917 and PRE2019-090730, and Unidad de Excelencia María de Maetzu under project MdM-2016-0692-17-2, the Xunta de Galicia grants GRC ED431C 2017/54 and ED431F2023/21 and a grant of the program Grupos de investigación consolidados (CIAICO/2022/008) financed by Generalitat Valenciana. Action co-financed by the European Union through the Programa Operativo del Fondo Europeo de Desarrollo Regional (FEDER) of the Comunitat Valenciana 2014–2020 (IDIFEDER/2021/002). This work was supported by 'la Caixa' Foundation (ID 100010434) (fellowship code LCF/BQ/PI20/11760027) and grant RYC2021-032654-I funded by MICIU/AEI/10.13039/501100011033 and by 'European Union NextGenerationEU'.

References

1. H. Daido, M. Nishiuchi, and A. S. Pirozhkov, Rep. Progress Phys. **75**, 056401 (2012).
2. A. Macchi, M. Borghesi, and M. Passoni, Rev. Mod. Phys. **85**, 751 (2013).
3. L. Robson, P. T. Simpson, R. J. Clarke, K. W. D. Ledingham, F. Lindau, O. Lundh, T. McCanny, P. Mora, D. Neely, C.-G. Wahlström, M. Zepf, and P. McKenna, Nat. Phys. **3**, 58 (2006).
4. J. Fuchs, P. Antici, E. d'Humières, E. Lefebvre, M. Borghesi, E. Brambrink, C. A. Cecchetti, M. Kaluza, V. Malka, M. Manclossi, S. Meyroneinc, P. Mora, J. Schreiber, T. Toncian, H. Pépin, and P. Audebert, Nat. Phys. **2**, 48 (2005).
5. A. Bembibre, A. Alejo, J. Peñas, and J. Benlliure, Eur. Phys. J. Web Conf. **290**, 08003 (2023).
6. J. T. Morrison, S. Feister, K. D. Frische, D. R. Austin, G. K. Ngirmang, N. R. Murphy, C. Orban, E. A. Chowdhury, and W. Roquemore, New J. Phys. **20**, 022001 (2018).
7. P. Poole, C. Andereck, D. Schumacher, R. Daskalova, S. Feister, K. George, C. Willis, K. Akli, and E. Chowdhury, Phys. Plasmas **21**, 063109 (2014).
8. D. Schumacher, P. Poole, C. Willis, G. Cochran, R. Daskalova, J. Purcell, and R. Heery, J. Instrum. **12**, C04023 (2017).
9. C. A. J. Palmer, N. P. Dover, I. Pogorelsky, M. Babzien, G. I. Dudnikova, M. Ispiriyan, M. N. Polyanskiy, J. Schreiber, P. Shkolnikov, V. Yakimenko, and Z. Najmudin, Phys. Rev. Lett. **106**, 014801 (2011).
10. P. Puyuelo Valdés, J. L. Henares, F. Hannachi, T. Ceccotti, J. Domange, M. Ehret, E. d'Humieres, L. Lancia, J.-R. Marquès, J. Santos, and M. Tarisien, Proc. SPIE **11037**, 110370B (2019).
11. A. Tebartz, S. Bedacht, M. Hesse, S. Astbury, R. Clarke, A. Ortner, G. Schaumann, F. Wagner, D. Neely, and M. Roth, Rev. Sci. Instrum. **88**, 093512 (2017).
12. J. Polz, A. P. L. Robinson, A. Kalinin, G. A. Becker, R. A. C. Fraga, M. Hellwing, M. Hornung, S. Keppler, A. Kessler, D. Klöpfel, H. Liebetrau, F. Schorcht, J. Hein, M. Zepf, R. E. Grisenti, and M. C. Kaluza, Sci. Rep. **9**, 16534 (2019).
13. T. Nayuki, Y. Oishi, T. Fujii, K. Nemoto, T. Kayoiji, Y. Okano, Y. Hironaka, K. G. Nakamura, K.-i. Kondo, and K.-i. Ueda, Rev. Sci. Instrum. **74**, 3293 (2003).
14. M. Noaman-ul Haq, H. Ahmed, T. Sokollik, L. Yu, Z. Liu, X. Yuan, F. Yuan, M. Mirzaie, X. Ge, L. Chen, and J. Zhang, Phys. Rev. Accel. Beams **20**, 041301 (2017).
15. F. P. Condamine, N. Jourdain, J.-C. Hernandez, M. Taylor, H. Bohlin, A. Fajstavr, T. M. Jeong, D. Kumar, T. Laštovička, O. Renner, and S. Weber, Rev. Sci. Instrum. **92**, 063504 (2021).
16. N. Xu, M. J. V. Streeter, O. C. Ettlinger, H. Ahmed, S. Astbury, M. Borghesi, N. Bourgeois, C. B. Curry, S. J. D. Dann, N. P. Dover, T. Dzelzainis, V. Istokskaia, M. Gauthier, L. Giuffrida, G. D. Glenn, S. H. Glenzer, R. J. Gray, J. S. Green, G. S. Hicks, C. Hyland, M. King, B. Loughran, D. Margarone, O. McCusker, P. McKenna, C. Parisuaña, P. Parsons, C. Spindloe, D. R. Symes, F. Treffert, C. A. J. Palmer, and Z. Najmudin, High Power Laser Sci. Eng. **11**, e23 (2023).
17. Y. Gao, J. Bin, D. Haffa, C. Kreuzer, J. Hartmann, M. Speicher, F. H. Lindner, T. M. Ostermayr, P. Hilz, T. F. Rösch, S. Lehrack, F. Englbrecht, S. Seuferling, M. Gilljohann, H. Ding, W. Ma, K. Parodi, and J. Schreiber, High Power Laser Sci. Eng. **5**, e12 (2017).
18. C. Spindloe, G. Arthur, F. Hall, S. Tomlinson, R. Potter, S. Kar, J. Green, A. Higginbotham, N. Booth, and M. K. Tolley, J. Phys. Conf. Ser. **713**, 012002 (2016).
19. R. Zaffino, M. Seimetz, D. Quirión, A. R. de la Cruz, I. Sánchez, P. Mur, J. Benlliure, L. Martín, L. Roso, J. M. Benlloch, M. Lozano, and G. Pellegrini, Microelectron. Eng. **194**, 67 (2018).
20. Y. Gershuni, D. Roitman, I. Cohen, E. Porat, Y. Danan, M. Elkind, A. Levanon, R. Louzon, D. Reichenberg, A. Tsabary, E. Urisman, S. Vaisman, and I. Pomerantz, Nucl. Instrum. Methods Phys. Res. A **934**, 58 (2019).
21. J. Benlliure, D. Cortina-Gil, J. Llerena, and C. Ruiz, Nucl. Instrum. Methods Phys. Res. Sect. A **916**, 158 (2019).
22. A. Alejo, A. Bembibre, J. Peñas, J. Benlliure, L. Martín, and M. T. Flores-Arias, Eur. Phys. J. Web Conf. **266**, 13001 (2022).
23. T. Chagovets, S. Stanček, L. Giuffrida, A. Velyhan, M. Tryus, F. Grepl, V. Istokskaia, V. Kantarelou, T. Wiste, J. C.

Hernandez Martin, F. Schillaci, and D. Margarone, Appl. Sci. **11**, 1680 (2021).
24. I. Alexeev, J. Wu, M. Karg, Z. Zalevsky, and M. Schmidt, Appl. Opt. **56**, 7413 (2017).
25. D. Carroll, M. Coury, G. Scott, P. McKenna, M. Streeter, H. Nakamura, Z. Najmudin, F. Fiorini, S. Green, J. Green, P. Foster, R. Heathcote, K. Poder, D. Symes, R. J. Clarke, R. Clarke, R. Pattathil, and D. Neely, "An assessment of the reproducibility of the Gemini retro focusing system," Central Laser Facility Annual Report (2011).
26. D. Kumar, M. Šmd, S. Singh, A. Soloviev, H. Bohlin, K. Burdonov, G. Fente, A. Kotov, L. Lancia, V. Lédl, S. Makarov, M. Morrissey, S. Perevalov, D. Romanovsky, S. Pikuz, R. Kodama, D. Neely, P. McKenna, T. Laštovička, M. Starodubtsev, S. Weber, M. Nakatsutsumi, and J. Fuchs, Matter Radiat. Extremes **4**, 024402 (2019).
27. P. K. Singh, K. Kakolee, T. W. Jeong, and S. Ter-Avetisyan, Nucl. Instrum. Methods Phys. Res. Sect. A **829**, 363 (2016).
28. M. Seimetz, P. Bellido, A. Soriano, J. García López, M. C. Jiménez-Ramos, B. Fernández, P. Conde, E. Crespo, A. J. González, L. Hernández, A. Iborra, L. Moliner, J. P. Rigla, M. J. Rodríguez-Álvarez, F. Sánchez, S. Sánchez, L. F. Vidal, and J. M. Benlloch, IEEE Trans. Nucl. Sci. **62**, 3216 (2015).

https://doi.org/10.1017/hpl.2024.13 Published online by Cambridge University Press